Earthquake history of the Milas Fault: An active dextral fault in an extensional province (SW Anatolia, Turkey)

Erdem KIRKAN (kirkan15@itu.edu.tr)
Istanbul Technical University: Istanbul Teknik Universitesi https://orcid.org/0000-0002-5229-1634
H. Serdar Akyüz
Istanbul Technical University: Istanbul Teknik Universitesi
Mehran Basmenji
Istanbul Technical University: Istanbul Teknik Universitesi
Aynur Dikbaş
İstanbul Üniversitesi-Cerrahpaşa: Istanbul Universitesi-Cerrahpasa
Cengiz Zabcı
Istanbul Technical University: Istanbul Teknik Universitesi
Müge Yazıcı
Helmholtz-Zentrum Potsdam GFZ: Deutsches Geoforschungszentrum Potsdam
M. Korhan Erturaç
Sakarya University: Sakarya Universitesi

Research Article

Keywords: The Milas Fault, earthquake, paleoseismology, SW Anatolia

Posted Date: March 31st, 2022

DOI: https://doi.org/10.21203/rs.3.rs-1131503/v1

Version of Record: A version of this preprint was published at Natural Hazards on January 2nd, 2023. See the published version at https://doi.org/10.1007/s11069-022-05733-w.

Abstract

The Milas Fault (MF) is a poorly known active fault located between the Büyük Menderes Graben to the north and the Gökova Graben to the south within the Anatolia-Aegean Region, SW Turkey. This dextral strike-slip fault has a length of 55 km between the Bafa Lake in the northwest and Çamlıca village in the southeast with a general strike of N60°W as its surface geometry displays two separate segments. We mapped the geomorphological and geological features of the MF by using Google Earth© images, Digital Elevation Models (DEMs) and field observations. The surface traces and kinematic characteristics of the MF are defined by rarely seen carbonate rocks, morphological lineaments and offsets streams, which all suggests a dominantly horizontal deformation for this peculiar tectonic structure. Moreover, we excavated three paleoseismological trenches in order to expose the signature of paleoearthquakes of the MF and to evaluate its seismic hazard potential. Evidences of three paleoearthquake events were revealed in trenches depending on the stratigraphical and structural relations of the exposed strata of latest Quaternary period. These earthquakes are dated as 1702±260 BC-2963±67 BC, 7152±600 BC-13502±3359 BC, and before 13502±3359 BC by means of combined OSL and ^{14}C dating results from youngest to oldest, respectively. These events are supposed to be around or larger than M 7.0 earthquakes. Even there is no constrained dates to propose recurrence interval, combined data from field observations, morphology, seismic records and paleoseismology indicate that the Milas Fault is an active structure and have a potential to produce a similar magnitude earthquake in the future.

1. Introduction

Neotectonics of Turkey is evolved with the commence of collisional convergence and tectonic escape-related deformation since the medial-late Miocene (Şengör et al. 1985). The convergent motions between the African, Arabian and Eurasian plates have deformed a region within the collisional sphere with acute impacts on the Anatolian Block (Şengör & Kidd 1979; Reilinger et al. 1997; Allen et al. 2004). The collision between the Arabian and the Eurasian plates along the Bitlis-Zagros Suture was followed by the escape of the Anatolian Block towards west between the sinistral East Anatolian Shear Zone (EASZ) and the right-lateral North Anatolian Shear Zone (NASZ) (Şengör 1980; Reilinger et al. 1997; Allen et al. 2004; Şengör & Yazıcı 2020). This escape is accelerated by the pull effect (back-arc spreading) of Hellenic Subduction in the western Anatolia (Barka & Reilinger et al. 1997; Bozkurt 2001; Reilinger et al. 2006). GNSS studies suggest a N-S regional extension with a rate of about 30-40 mm/yr. in the western Anatolia (Reilinger et al. 1997; Kreemer et al. 2014), which is defined as the Western Anatolian Extensional Province (WAEP) (Fig. 1a).

The WAEP forms one of the unique active extensional regions in the world (Jackson & McKenzie 1988; Reilinger et al. 1997; Taymaz & Jackson 1991; Bozkurt 2001). The general framework of this system is governed by the E-W trending normal faults (e.g. Edremit, Bakırçay, Kütahya, Simav, Gediz, Büyük Menderes and Gökova grabens). The geodetic studies (McClusky et al. 2003; Reilinger et al. 1997) reveal that the general N-S extension in the WAEP indicate that there must be a more complex evolution between Büyük Menderes Graben (BMG) and Gökova Fault Zone (GFZ), represented by the NE-SW trending Söke normal fault, NW-SE trending Muğla-Yatağan normal faults (Emre et al. 2013) and the NW-SE trending dextral Milas Fault (MF) (Fig. 1b). The distribution of total strain between the BMG and GFZ is quite complicated; therefore, detailed studies such as GNNS, paleomagnetism, seismology and tectonostratigraphy are needed to solve this problem. In this study, we study the activity of the MF, as being one of the major structures of this complex region, by investigating its paleoseismic history. Milas province is a rapidly growing and urbanizing region due to its fertile agricultural lands, tourism potential and preferable climate conditions. Therefore, determining a possible earthquake risk is of utmost importance for this region. Historical earthquake records and paleoseismologic studies demonstrate that the SW Anatolia hosted numerous earthquakes during the late Holocene (Papazachos et al. 1991; Guidoboni 1994; Ambraseys & Jackson 1998; Guidoboni et al. 2005; Karabacak 2016;

Basmenji et al. 2021). Among these extensive historical records, there is no clear data on the place of the MF in the seismicity of the SW Anatolia. Any evidence for past earthquakes on the MF will not provide information on the seismic hazard for this region, but it will also contribute to our understanding in such complex extensional regions elsewhere in the world.

2. Materials & Methods

Paleoseismic trenching is one of the most practical methods providing a good overview about seismic history of active faults. The focus of this method is to determine earthquake cycles related to the individual fault systems and provide insights about cumulative surface slip associated with past earthquakes along the identical system (McCalpin 2009). Therefore, paleoseismology along with geomorphological investigations cater the most reliable information regarding the seismic hazard evaluations (McCalpin 2009; Meghraoui & Atakan 2014). Determination of recurrence intervals of earthquakes with short return periods is possible with correlation of paleoseismological dataset e.g. (Schwartz & Coppersmith 1984; Thatcher 1984; Sieh et al. 1989; Thatcher 1990; Goes 1996; Weldon et al. 2004; Dolan et al. 2007; Rockwell et al. 2009; Akyüz et al. 2015).

To identify the structural and morphologic properties and generate a detailed map of the Milas Fault (MF); we used Advanced Spaceborne Thermal Emission and Reflection Radiometer (ASTER) DEMs (30m ground pixel resolution), Google Earth images and Unmanned Air Vehicle (UAV) photos, which are used to produce high resolution digital surface models (DSM) and orthophotographs as well. Morphotectonic features such as fault scarps, offset gullies, morphological lineaments and scarps, in addition to geological and stratigraphic relations of units are defined in the field along the entire MF. All data were compiled and processed in the ArcGIS software.

Paleoseismological trench study includes site selection, excavation, trench preparation, sampling, logging, dating and interpretation stages. Potential trench locations were determined based on Google Earth images and suitable ones were selected for trenching by field investigations. All of the trenches were excavated perpendicular to the main trend of the fault and trench positions recorded by using a handheld Garmin GPS Map 60. We followed the methodology as described by (Akyüz et al. 2015) for the preparation and logging the trench walls. For which, trench walls were manually cleaned using by hand tools and gridded (1×1 m) to identify and log the faults, related structures, and the stratigraphic units. All trench walls were logged in a scale of 1:20 and we also correlated our logs with the photomosaics of the trench walls. The field data were digitized to finalise trench logs. Samples from critical levels were collected for radiocarbon (^{14}C) and Optically Stimulated Luminescence (OSL) dating. Quartz crystals from OSL sample tubes were extracted in MALTA Lab. (Sakarya University, Turkey). Luminescence tests and De measurements from 16 aliquots were performed using a Risø TL/OSL Reader DA-20 equipped with $^{90}Sr/^{90}Y$ (0.13 ± 0.04 Gy/s) source installed at the Ankara University Institute of Nuclear Sciences, Luminescence Research and Dating Laboratory. Geochemical analysis of the radioactive elements (U, Th, K, and Rb) was conducted at the accredited ALS-Global Laboratory (Canada), using inductively coupled plasma mass spectroscopy (ICP-MS) for trace elements (ALS Code: ME-MS81) and inductively coupled atomic emission spectroscopy (ICP-AES) for major oxides (ALS Code: MEICP06). Environmental Dose rate and age of each sample is calculated by using DRc software (Tsakalos et al. 2016). Further details of the procedure and instrumentation is described in (Erturaç et al. 2019). Bulk and charcoal samples were analysed in Poznan Radiocarbon Lab. ^{14}C results were calibrated by OxCal (Bronk Ramsey and Lee 2013), using the correction curves by (Reimer et al. 2013).

3. The Milas Fault: Its Geology, Morphology, Segmentation And Seismic History

3.1 Geology

The Milas Fault (MF) prolongs along the Milas-Karakuyu Basin which covers the lithological units of different ages overlying the southern Menderes Massif (Okay 1989; Gürer & Yılmaz 2002; Bozkurt 2007). Selimiye Formation is the oldest unit in the region around the MF (Dürr 1975) (Fig. 2). The Selimiye Formation is considered within the core complex of the Menderes Massif (Hetzel & Reischmann 1996; Loos S & Reischmann 1999; Gessner et al. 2004); however, unlike other parts of the Menderes Massif, the Selimiye Formation has undergone metamorphism in the Neoproterozoic; the cooling ages determined from the metagranitoids are of Eocene age (Bozkurt & Satir 2000; Candan et al. 2001). The formation consists of micaschists and highly foliated phyllites. In addition, there are thin marbles with lenticular geometry, sometimes making lateral and vertical transitions or having sharp contacts with other units at different levels (Aksoy 2004). Selimiye Formation is overlain by the Permo-Carboniferous Göbektepe Formation, which consists of thick bedded dark coloured phyllite, recrystallized limestones and quartzites. Limestones are dated by using foraminifers as Permo-Carboniferous (Önay 1949; Çağlayan et al. 1980; Okay et al. 2001). The Göktepe Formation is stratigraphically overlain by a Mesozoic aged thick carbonate unit called the Milas marble that is mainly made up of platform-type massive carbonates of rudist-bearing marbles, intraformational carbonate breccias and marbles with chert intercalations from the bottom to the top (Dürr 1975; Özer 1998). Miocene detritic sediments cover the Milas marble unconformably in the south of the Beçin village. All these units are covered by Quaternary alluviums along the Milas-Karakuyu Basin (Fig. 2).

3.2 Morphology and segmentation

The MF is one of the active tectonic structures in southwestern Anatolia located between the Büyük Menderes Graben and Gökova Fault Zone. The MF has a 55 km length with the strike of N60°W between the Bafa Lake and Çamlıca Village and has a dominant right lateral strike-slip movement with slight vertical component (Fig. 3). There are limited studies about the structural characteristics of the fault. The MF was mapped as a possible active fault first by Şaroğlu et al. (1987) and defined as the “Karaova – Milas Fault Zone”. Later, the MF were classified as two segments of a right-lateral strike-slip fault and named by Emre et al. (2013) as; Karakuyu to the northwest and Beçin to the southeast. Although information on the location and geometry of the fault has been recorded in previous studies (Emre et al. 2013; Karabacak 2016), there are limited data on its actual tectonic activity and seismogenic characteristics. The MF is an important structure because there are some dense populated towns and villages along it. Even it is defined as an active fault, its detailed geometry, morphotectonic indicators and recent tectonic activity is unknown. The detailed mapping of the active faults provides a dataset that include evolution of the structural, morphological and lithological variations (e.g. orientation and geometry, ground ruptures, fault scarps and deformation setting) sourced by the tectonically active landscapes and these variations are significant to detect the affiliation of earthquakes potential (McClay 2013). Generally, the fault map prepared in this study represents similar geometry to the active fault map of (Duman et al. 2011) and (Emre et al. 2013), with some differences in detail and in the NW and SE ends of the fault.

The MF consists of two segments which are separated with a 3,5 km-wide releasing step-over around the Milas Town with a N-S striking normal fault linking these two segments. The western, Karakuyu, segment has 30 km length while the eastern one, Beçin, has a length of 25 km (Emre et al. 2013). The Karakuyu Segment trends between south of the Bafa Lake and the Milas City, running through a high relief within the Milas marble for 12 km between Hisarcık and Karakuyu villages. Beçin Segment prolongs for ~25 km between the Beçin Village at SE of the Milas City center and the Çamlıca Village to southeast. To the west of Beçin, it forms a boundary between Quaternary deposits in the Milas Basin and the Miocene clastics to the south. The fault cuts through the Milas marbles (Mesozoic) between the

Aslanyaka and Kalınağıl villages. To the south of the Kalınağıl Village, the Beçin Segment shows some parallel branches towards southeast within the Milas marble. The fault trace ends around the Çamlıca Village after making a lazy bend to left.

Fault planes in marbles were detected at limited locations. A spectacular one is in the Pınarcık Village on the Karakuyu Segment. The fault plane exposure is about 20 meters high in marbles (Fig. 4a) where fault slicken-lines could not be observed due to high alteration and erosion. The western extend of this exposure (~200 m) indicate a right-lateral oblique motion of the MF with a rake angle of 24° (Fig. 4b).

As a result of the curved geometry close to both ends of the MF, small fault splays at NW and SE develop as “horsetail” structures at the end points of the MF. The late Quaternary tectonic activity of the MF is mainly characterised with a linear trough and dextrally offset channels from 40 to 100 of meters (Figs. 4c, d, e, and f).

3.3 Seismic history

Instrumental seismicity and historical seismic records indicate that there have been some moderate-magnitude earthquakes along the MF (Fig. 3).

A single historical event that can be associated with the MF is the 1631 AD Beçin Earthquake (Ambraseys 2009). The governor of Beçin, who kept the historical records in the region, explained that the walls of the salt stores in the Milas and Beçin were damaged due to the 1631 event. There is no mention of any casualties or any detailed and large destruction related to this earthquake. For this reason, we interpreted that the 1631 event was not a surface rupturing earthquake.

We also compiled earthquake records that have occurred between 1940 and 2020 and classified them by using different databases and publications (Ambraseys & Jackson 1998; Ersoy et al. 2000; Kadirioğlu et al. 2018; AFAD; ISC; KOERI; NEIC). There are two major earthquakes occurred at the eastern end of the Beçin Segment at 19:51 and 22:34 on 23.05.1941 with magnitude M_s=6 and M_s=5.6, respectively (Table 1; Fig. 3). During these earthquakes, 3 people died and 7 people were injured because of fallen blocks and collapsed houses. A total of 25 houses in Milas and Muğla were severely damaged and 5 buildings were completely destroyed (DABCA). There is no reported surface rupture caused by these earthquakes.

Table 1
List of instrumental earthquakes in the study area (a: Ambraseys & Jackson 1998, b: Ersoy et al 2000, c: Kadirioğlu et al 2018, AFAD: Disaster & Emergency Management Authority Presidential of Earthquake Department, ISC: International Seismological Centre, KOERI: Kandilli Observatory and Earthquake Research Institute, NEIC: USGS National Earthquake Information Center.)

No	Date	Lat.	Long.	Depth (Km)	M Type	Magnitude	References
1	23.05.1941	37.25	28.00	35.0	M_s	6.0	a, b, c
2	23.05.1941	37.25	28.00	35.0	M_s	5.6	a, b, c
3	19.07.1971	37.50	27.40	16.0	M	4.0	KOERI
4	27.12.1988	37.38	27.63	10.0	M_d	4.1	AFAD
5	20.05.1996	37.41	27.52	12.0	M_d	4.1	ISC
6	26.05.2019	37.23	28.02	10.0	M_d	4.5	NEIC

4. Paleoseismology Of The Milas Fault

Paleoseismic trenching is the most common technique that provides information about the time, size and location of past earthquakes and investigates the future seismic potential of any fault (McCalpin 2009). To explore the seismic history and earthquake potential of the MF, we excavated three fault-perpendicular trenches (Ağılyanı-1 and 2, and Zeytinlik trench) (Fig. 5) at two different sites on the Karakuyu Segment. Trench sites were determined based on the fault morphology, suitable depositional environment for Holocene sedimentation, low level of underground water and convenient logistic conditions.

4.1 Ağılyanı-1 trench

The Ağılyanı-1 trench is located at Gümüşlük district, approximately ~2 km west of the Milas Town. This site is located on a linear saddle morphology. Recent sedimentation is mainly made of fine siliciclasts, which are sourced from the southern slopes and seasonal gullies. The trench is 13 m in length, 1.5 m in width and about 2.5 m in depth (Fig. 6).

The trench exposure starts with the greenish-grey mica schists at the bottom (Unit-V; Fig. 7). Unit IV, made of silt with gravel and blocks, unconformably overlies the Unit-V, whereas light brown silt with rare sand and clay (Unit-III) covers all units below between 0 and 6th meters. The upper part of the trench exposure is represented with the light grey silt with gravels (Unit I) and various silts with coarse sand or gravels (Units II and IIa) exposing a clear erosional contact at the bottom of the sequence.

The most prominent structural feature is a 1-meter-wide fault zone between 8th to 9th meters, which is characterised by sharp vertical contacts including parallel-subparallel fault branches (Figs. 7 and 8). These faults cut the basement rock (Unit-V) together with secondary fault branches in 7th and 10th meters. This zone and secondary faults are covered by sandy/pebbly/silty deposits (Unit II and I) on an erosional surface that represents the last event horizon (E-1). Fine grained infill material within the main fault zone are also cut by faults and includes shear fabric along these structural features (Fig. 8). This infill is an indicator for an earthquake and postdate Event-2 (E-2). At the bottom of this zone, it is seen that a couple of vertical fault branches were covered with silty sand which is interpreted as the oldest event horizon (E-3) (Fig. 7).

We collected four samples for OSL dating to constrain the timing of past earthquakes in the Ağılyanı-1 trench (Tables 2 and 3). Sample AGL1-O1 was taken from lower part of the Unit-II that emplaced on an erosional surface on the main fault zone between 8th and 9th meters and yielded 232±260 BC giving the depositional age of the sedimentary layer covering an event (Event-1). AGL1-O3 was taken within the main fault zone that represents the date of infill material providing a post-date of an earthquake as 7152±660 BC. Another clue for penultimate event is the tilted Unit-IV located on another erosional surface on the northern end of the basement. The OSL date (AGL1-O9) from Unit IV (7110±153 BC) is convenient with the infill date and supports the post-date of the penultimate event (Event-2). At the bottom part of main fault zone, it is observed that a couple of fault branches were covered by greenish yellow sandy silt. The OSL date (AGL1-O4) from bottom part of this stratum gives another postevent date of 13502±3359 BC (Event-3). Even there is no any pre-date restrictions for past earthquakes in this trench, we can conclude that there are three surface-rupturing earthquake evidences in this trench two of which has occurred during the Holocene.

Table 2
Variables for OSL dates from Ağılyanı-1, Ağılyanı-2 and Zeytinlik Trenches. All ages represent year before 2018 which are further calibrated to chronological age (BC) accordingly

Sample	U (ppm)	Th (ppm)	Rb (ppm)	K (%)	Equivalent Dose (Gy)	Cosmic Dose Rate (Gy/ka)	Environmental Dose Rate (Gy/ka)	OSL Age (ka)	Chronological Age (BC)
AGL1-O1	2.93	10.10	76.80	1.89	7.00 ± 0.81	0.164	3.106 ± 0.03	2.25 ± 0.26	232 ± 260
AGL1-O3	2.45	13.50	105.50	2.58	34.9 ± 2.5	0.134	3.804 ± 0.039	9.17 ± 0.66	7152 ± 660
AGL1-O4	1.87	11.15	110.50	2.91	60.07 ± 13	0.13	3.87 ± 0.023	15.52 ± 3.359	13502 ± 3359
AGL1-O9	2.54	10.65	87.70	2.17	30.00 ± 0.4	0.142	3.286 ± 0.033	9.129 ± 0.153	7110 ± 153
AGL2-O2	2.40	12.35	91.80	2.24	10.2 ± 0.7	0.149	2.74 ± 0.03	3.72 ± 0.26	1702 ± 260

Table 3
Radiocarbon Dates from Ağılyanı-1, Ağılyanı-2 and Zeytinlik Trenches

Sample	Laboratory ID No	Material type and weight (mg)	Radiocarbon age (BP)	2σ Calibrated age (BC)	Chronological age (BC)
AGL2-B3	Poz-109420	Organic Sediments (0.3)	4350 ± 35	3030-2896 (89.8%)	2963 ± 67
ZY- B2	Poz-102782	Organic Material (0.3)	3335 ± 35	1694-1526 (92.9%)	1610 ± 84

4.2 Ağılyanı-2 trench

Ağılyanı-2 Trench was excavated 50 m to the west of Ağılyanı-1, which is 16 m in length, 1.5 m in width and 3 m in depth. The sequence starts with green schists (Unit-VIII), at the bottom, which is overlain by Unit-VII of altered bedrock to the south of the trench wall, between 0th to 6th meters. The upper stratigraphic layers on the southernmost part are mainly composed of slope-wash deposits of fine grained and dark coloured silts and clays. These strata had been excavated and filled by artificial material between 0th to 5th meters. Between 5th -16th meters the bottommost layers were cut by channels of various sizes. The upper layers are represented by silt, coarse sand and gravel and they lay almost horizontal along the trench wall. At the northern part of the trench; schists (Unit-VIII) are covered with brownish sandy-clay (Unit-V), dark brown silty-clay (Unit-IV), light brown silt with gravel (Unit-III), clay with grey sand and gravel (Unit-II), and coarse sand with thin sand bands and sand lenses (Unit-I) (Fig. 9).

At the bottom of the trench; around 3th meter, the faulted bedrock units (Unit-VII and Unit-VIII) were blanked by a brown clay layer after an erosional period (Unit-VI) (Fig. 10). Another fault branch which belongs to same event were found at the 11th meter of the trench base which cuts the bedrock, but is covered with the sandy clay unit (Unit V). We sampled the layer above the event horizon for OSL (AGL2-O2) and radiocarbon (AGL2-B3) dating (Tables 2 and 3),

which respectively yield between 1702±260 BC and 2963±67 BC which is comparable with the Event-1 in the Ağılyanı-1 trench.

4.3 Zeytinlik trench

Zeytinlik Trench is located on a linear escarpment within the continuation of the morphological saddle structure of the Ağılyanı Site (Fig. 11). Trench has a 17 m length, 1.5 m width and 2.5 m depth. It is located on the southeastern part of the Karakuyu segment (~ 1,5 km west of Milas city center) and 1 km southeast of Ağılyanı trench site.

The stratigraphy of the trench is represented with typical colluvium deposits, which are derived from the southern slopes and mostly made of coarse-grained and angular marble pebbles and blocks with a clay-silt-sand matrix. There are abundant caliche formations within the matrix. We identified a total of five units within the stratigraphy of the trench. The oldest unit (Unit-V) in the trench is a sand layer with dark brown clay matrix containing angular pebbles and gravels (Fig. 12). The Unit-V is conformably overlain by brown sandy clay with angular blocks (Unit-IV) and gravel with brown clay matrix (Unit-III). These units slightly dip to the south.

Between the 11th and 15th meters, the layers (Unit-V, Unit-IV and Unit-III) are cut and displaced by parallel/sub-parallel faults. Especially at 12th m meter, an infill is observable between these fault branches (Fig. 13).

The upper termination of fault branches is covered with the dark yellow sandy silt (Unit-II). This unit is continuous throughout the trench wall and is emplaced on an erosional surface. The youngest layer (Unit-I) is reddish brown clay layer which comprises rare gravel and blocks. The thickness of the Unit-I is noticeably high in the north and it wedges to the south end of the trench. A single radiocarbon sample from Unit-II (ZY-B2) yields age of 1610 ± 84 BC, which postdates the event horizon of the Zeytinlik Trench. This is also comparable with the Event-1 of Ağılyanı-1 and -2 trenches.

5 Discussion And Conclusion

The MF is a NW-SE striking dextral fault in SW Turkey. In order to unravel the characteristic features of the MF and evaluate the earthquake activity through the Holocene, we constructed a detailed multi-disciplinary study containing morphological and structural observations for paleoseismological perspective. The MF's effect on the geomorphological evolution of the area have been investigated by using DEM images and field surveys. The MF strikes mostly through the basement rocks forming a high-relief morphology, while it bounds the Quaternary basin in places. Dextral stream offsets of ranging between 40 and 100 m are observed along the Karakuyu Segment. There are *en échelon* faults, showing a typical horsetail structure on the NW and SE terminations of the MF. Other significant morphological features are the linear troughs that are located between the Milas City centre and the southeast edge of the Karakuyu Segment.

Joint analyses of remote sensing and field surveys have allowed us to prepare a precise map of the MF. Based on these, we selected the paleoseismic trench sites in order to investigate the earthquake history of the MF. Three trenches represented in this study are the first paleoseismic excavations on the MF. The faulted Holocene strata were defined in all trenches. Combining dating results, we revealed three different surface-rupturing earthquake events, among two have happened during the Holocene (Fig. 14). The oldest event should have occurred before 13500 BC while the penultimate one ruptured the fault in between 13500 BC and 7152 BC. The youngest event that produced the surface rupture is dated between 1702±260 BC and 2963±67 BC.

There is very limited data about historical earthquakes directly related to the MF. A major historical earthquake at the Beçin region (1631 AD) have been documented by (Ambraseys 2009) Some damage on the buildings and the salt

depots have been recorded by the governor of the Beçin. Even though there are damage on the building and the constructions, there is no record in terms of casualties and economical loss. Due to this ambiguous and weak documentation and the absence of the fault rupture on the surface, 1631 earthquake could be interpreted as a moderate event and did not produce any surface rupture. In instrumental period, the most significant earthquakes occurred in 23 May 1941 on the Beçin Segment of the MF. In the same day, there were two earthquakes; M_s=5.6 and M_s=6.0 (Ambraseys & Jackson 1998; Ersoy et al. 2000; Kadirioğlu et al. 2018). According to the instrumental records, a total of 44 M=3.5-3.9 and 6 M>4 earthquakes have been recorded between 1900 and 2020 (Table 1). When the scarce seismicity of the Milas Region is compared with the dense seismicity of the SW Anatolia, a relatively slow tectonic motion is taking place at the Milas region in terms of earthquake activity. In order to calculate the numerical earthquake productivity of the MF, an empirical function (MAG=1.12 × LOG RL + 5.16, where RL represents the rupture length) of the (Wells & Coppersmith 1994) have been considered. Two possible scenarios were integrated and their maximum intensity is interpolated; Karakuyu and Beçin segments can be broken as separate segments or together. If the segments might produce discrete earthquakes, Karakuyu and Beçin segments could produce M=6.8 and M=6.6 earthquakes, respectively. Moreover, these interpretations are compatible with the similar result of (Emre et al. 2018) which have calculated M=6.7 and M=6.6 for these segments. If two segments rupture together then it may produce a M=7.1 earthquake. The evidence for surface faulting in our trenches and clear fault-related morphology suggest that it is more likely to have a M≥7, generating a surface rupture along the entire length of the MF, which should be considered is seismic hazard assessments for the region.

Declarations

Acknowledgement

This study is a part of the Erdem Kırkan's MSc thesis. The authors thank to Dr. Eren Şahiner and Dr. Niyazi Meriç for OSL dating. Enver Sürmeli and Beste Karatepe are thanked for assistance during the field studies. Comments and fruitful discussions with, Dr. Gülsen Uçarkuş, Nurettin Yakupoğlu and Asen Sabuncu improved an initial draft of the manuscript. Thanks to Dr. M. Ersen Aksoy for useful discussions in the field and photograph of trench walls. Some figures in this paper were generated by Generic Mapping Tools (GMT).

Funding

This work was supported by Scientific and Technological Research Council of Turkey-TUBITAK (Grant number 116Y179).

Conflict of interest

The authors declare that they have no conflict of interest.

References

1. Akbaş B, Akdeniz N, Aksay A, Altun İ, Balcı V et al (2011) Geological Map of Turkey, General Directorate of Mineral Reserach and Exploration Publications. Ankara-Turkey
2. Aksoy R (2004) Selimiye (Milas, Muğla) Kuzeyinde Menderes masifinin mesoskopik tektonik özellikleri. Selçuk Üniversitesi Mühendislik. Bilim ve Teknoloji Dergisi 19(2):61–68
3. Akyüz HS, Karabacak V, Zabcı C (2015) Paleoseismic trenching. Encyclopedia of Earthquake Engineering. Springer Publications. https://doi.org/10.1007/978-3-642-36197-5_107-1

4. Allen M, Jackson J, Walker R (2004) Late Cenozoic reorganization of the Arabia-Eurasia collision and the comparison of short-term and long-term deformation rates. Tectonics 23(2). https://doi.org/10.1029/2003TC001530
5. Ambraseys N (2009) Earthquakes in the Mediterranean and Middle East: a multidisciplinary study of seismicity up to 1900. Cambridge University Press
6. Ambraseys N, Jackson JA (1998) Faulting associated with historical and recent earthquakes in the Eastern Mediterranean region, Geophysical Journal International, vol UK., 133(Blackwell Publishing Ltd Oxford, pp 390–406. 2https://doi.org/10.1046/j.1365-246X.1998.00508.x
7. Barka A (1992) The north Anatolian fault zone. In Annales tectonicae (Vol. 6, No. Suppl, pp. 164-195)
8. Barka A, Reilinger R (1997) Active tectonics of the Eastern Mediterranean region: deduced from GPS, neotectonic and seismicity data. Annals of Geophysics XL 587–610. https://doi.org/10.4401/ag-3892
9. Basmenji M, Akyüz HS, Kirkan E, Aksoy ME, Uçarkuş G, Yakupoğlu N (2021) Earthquake history of the Yatağan Fault (Muğla, SW Turkey): implications for regional seismic hazard assessment and paleoseismology in extensional provinces. Turkish Journal of Earth Sciences 30(2). https://doi.org/10.3906/yer-2006-23
10. Bozkurt E, Satir M (2000) The southern Menderes Massif (western Turkey): geochronology and exhumation history. Geol J 35(3–4):285–296. https://doi.org/10.1002/gj.849
11. Bozkurt E (2001) Neotectonics of Turkey–a synthesis. Geodin Acta 14(1–3). 3-30 .. https://doi.org/10.1080/09853111.2001.11432432
12. Bozkurt E (2007) Extensional v. contractional origin for the southern Menderes shear zone, SW Turkey: tectonic and metamorphic implications. Geol Mag 144(1):191–210. https://doi.org/10.1017/S0016756806002664
13. Çağlayan MA, Öztürk EM, Öztürk Z, Sav H, Akat U (1980) Menderes Masifı güneyine ait bulgular ve yapısal yorum. Jeoloji Mühendisliği 10:9–19. (in Turkish with English abstract).
14. Candan O, Dora O, Oberhänsli R, Cetinkaplan M, Partzsch J, Warkus F, Dürr S (2001) Pan-African high-pressure metamorphism in the Precambrian basement of the Menderes Massif, western Anatolia, Turkey. Int J Earth Sci 89(4):793–811. https://doi.org/10.1007/s005310000097
15. Devlet Arşivleri Başkanlığı Cumhuriyet Arşivi (DABCA) 030.10.119.847.3
16. Dolan JF, Bowman DD, Sammis CG (2007) Long-range and long-term fault interactions in Southern California. Geology 35(9):855–858
17. Duman TY, Emre Ö, Özalp S, Elmacı H (2011) 1: 250,000 scale active fault map series of Turkey, Aydın (NJ 35-11) Quadrangle. General Directorate of Mineral Reserach and Exploration Publications. General Directorate of Mineral Research and Exploration, Ankara, Turkey
18. Dürr S (1975) Über Alter und geotektonische Stellung des Menderes-Kristallins, SW Anatolien und seine Aequivalente in der Mittleren Aegaeis: Thesis, Marburg, Lahn, West Germany (in German)
19. Emre Ö, Duman TY, Özalp S, Elmacı H, Olgun Ş et al (2013) Açıklamalı Türkiye Diri Fay Haritası Ölçek 1/1.125. 000: Maden Tetkik ve Arama Genel Müdürlüğü Özel Yayın Serisi 30, Special Publication Series of MTA-30.
20. Emre Ö, Duman TY, Özalp S, Şaroğlu F, Olgun Ş, Elmacı H, Can T (2018) Active fault database of Turkey. Bull Earthq Eng 16(8):3229–3275. https://doi.org/10.1007/s10518-016-0041-2
21. Ersoy Ş, Altınok Y, Yalçıner AC (2000) Güneybatı Anadolu'nun Neotektonik Yapılarına Genel bir bakış ve bölgenin deprem etkinliği, III. Ulusal Kıyı Mühendisliği Sempozyumu-Çanakkale, Çanakkale, Türkiye, 05 Ekim 2000, cilt.1, ss.115-128

22. Erturaç MK, Şahiner E, Zabcı C, Okur H, Polymeris GS, Meriç N, İkiel C (2019) Fluvial response to rising levels of the Black Sea and to climate changes during the Holocene: Luminescence geochronology of the Sakarya terraces. The Holocene 29(6):941–952. https://doi.org/10.1177/0959683619831428
23. Gessner K, Collins AS, Ring U, Güngör T (2004) Structural and thermal history of poly-orogenic basement: U–Pb geochronology of granitoid rocks in the southern Menderes Massif, Western Turkey. J Geol Soc 161(1):93–101. https://doi.org/10.1144/0016-764902-166
24. Global CMT (ed) https://www.globalcmt.org/CMTsearch.html (acessed 03.06.2021)
25. Goes SD (1996) Irregular recurrence of large earthquakes: an analysis of historic and paleoseismic catalogs. Journal of Geophysical Research: Solid Earth 101(B3):5739–5749. https://doi.org/10.1029/95JB03044
26. Guidoboni E, Comastri A, Boschi E (2005) The “exceptional” earthquake of 3 January 1117 in the Verona area (northern Italy): A critical time review and detection of two lost earthquakes (lower Germany and Tuscany). Journal of Geophysical Research: Solid Earth 110(B12). https://doi.org/10.1029/2005JB003683
27. Guidoboni E, Comastri A, Traina G, Geofisica RIN (eds) (1994) Catalogue of Ancient Earthquakes in the Mediterranean Area up to the 10th Century, 1st edn. Istituto Nazionale di Geofisica e Vulcanologia, Rome, Italy
28. Gürer ÖF, Yılmaz Y (2002) Geology of the Ören and surrounding regions, SW Turkey. Turkish Journal of Earth Sciences 11:2–18
29. Hetzel R, Reischmann T (1996) Intrusion age of Pan-African augen gneisses in the southern Menderes Massif and the age of cooling after Alpine ductile extensional deformation. Geol Mag 133(5):565–572. https://doi.org/10.1017/S0016756800007846
30. Jackson J, McKenzie D (1988) Rates of active deformation in the Aegean Sea and surrounding regions. Basin Res 1(3):121–128. https://doi.org/10.1111/j.1365-2117.1988.tb00009.x
31. Kadirioğlu FT, Kartal RF, Kılıç T, Kalafat D, Duman TY et al (2018) An improved earthquake catalogue (M≥ 4.0) for Turkey and its near vicinity (1900–2012), Bulletin of Earthquake Engineering, vol 16. Springer, pp 3317–3338. 8https://doi.org/10.1007/s10518-016-0064-8
32. Karabacak V (2016) Seismic damage in the Lagina sacred area on the Mugla Fault: a key point for the understanding of the obliquely situated faults of western Anatolia. J Seismolog 20(1):277–289. https://doi.org/10.1007/s10950-015-9526-8
33. Kiratzi A, Louvari E (2003) Focal mechanisms of shallow earthquakes in the Aegean Sea and the surrounding lands determined by waveform modelling: a new database. Journal of Geodynamics Elsevier 36(1–2):251–274. https://doi.org/10.1016/S0264-3707(03)00050-4
34. Kreemer C, Blewitt G, Klein EC (2014) A geodetic plate motion and Global Strain Rate Model, Geochemistry, Geophysics, Geosystems. Wiley Online Library 15(10):3849–3889. https://doi.org/10.1002/2014GC005407
35. Loos S, Reischmann T (1999) The evolution of the southern Menderes Massif in SW Turkey as revealed by zircon dating. J Geol Soc 156(5):1021–1030. https://doi.org/10.1144/gsjgs.156.5.1021
36. McCalpin JP (ed) (2009) Paleoseismology. Academic press
37. McClay KR (2013) The mapping of geological structures. John Wiley & Sons
38. McClusky S, Reilinger R, Mahmoud S, Ben Sari D, Tealeb A (2003) GPS constraints on Africa (Nubia) and Arabia plate motions. Geophysical Journal International Blackwell Publishing Ltd Oxford, UK 155(1):126–138. https://doi.org/10.1046/j.1365-246X.2003.02023.x
39. Meghraoui M, Atakan K (2014) The contribution of paleoseismology to earthquake hazard evaluations. In Earthquake Hazard, Risk and Disasters (pp. 237-271). Academic Press. https://doi.org/10.1016/B978-0-12-394848-9.00010-9

40. Okay AI (1989) Denizli'nin güneyinde Menderes masifı ve Likya naplarının jeolojisi. General Directorate of Mineral Reserach and Exploration Publications.Ankara-Turkey, 109(109)
41. Okay AI (2008) Geology of Turkey: a synopsis. Anschnitt 21:19–42
42. Okay AI, Tansel I, Tuysuz O (2001) Obduction, subduction and collision as reflected in the Upper Cretaceous–Lower Eocene sedimentary record of western Turkey. Geol Mag 138(2):117–142. https://doi.org/10.1017/S0016756801005088
43. Önay T (1949) Ueber die Smirgelgesteine Südwest-Anatoliens. Schweiz Mineral Petrogr Mitt 29:359–484. https://doi.org/10.3929/ethz-a-000103756
44. Özer S (1998) Rudist bearing Upper Cretaceousmetamorphic sequences of the Menderes Massif (Western Turkey). Geobios 31:235–249. https://doi.org/10.1016/S0016-6995(98)80080-6
45. Papazachos B, Kiratzi A, Papadimitriou E (1991) Regional focal mechanisms for earthquakes in the Aegean area. Source Mechanism and Seismotectonics. Birkhäuser, Basel, pp 405–420. https://doi.org/10.1007/978-3-0348-8654-3_4
46. Ramsey CB, Lee S (2013) Recent and planned developments of the program OxCal. Radiocarbon 55(2–3):720–730
47. Ramsey CB (2020) "OxCal 4.3 Manual," https://c14.arch.ox.ac.uk/oxcalhelp/hlp_contents.html
48. Reilinger RE, McClusky S, Vernant P, Lawrence S, Ergintav S, Cakmak R, Nadariya M (2006) GPS constraints on continental deformation in the Africa-Arabia-Eurasia continental collision zone and implications for the dynamics of plate interactions. Journal of Geophysical Research: Solid Earth 111(B5). https://doi.org/10.1029/2005JB004051
49. Reilinger RE, McClusky SC, Oral MB, King RW, Toksoz MN, Barka AA, Sanli I (1997) Global Positioning System measurements of present-day crustal movements in the Arabia-Africa-Eurasia plate collision zone. Journal of Geophysical Research: Solid Earth 102(B5):9983–9999. https://doi.org/10.1029/96JB03736
50. Reimer PJ, Bard E, Bayliss A, Beck JW, Blackwell PG et al (2013) IntCal13 and Marine13 radiocarbon age calibration curves 0–50,000 years cal BP, Radiocarbon. Cambridge University Press 55(4):1869–1887. https://doi.org/10.2458/azu_js_rc.55.16947
51. Rockwell T, Ragona D, Seitz G, Langridge R, Aksoy ME, Ucarkus G et al (2009) Palaeoseismology of the North Anatolian Fault near the Marmara Sea: implications for fault segmentation and seismic hazard. Geological Society, London, Special Publications, 316(1), 31-54. https://doi.org/10.1144/SP316.3
52. Şaroğlu F, Boray A, Emre Ö (1987) Active faults of Turkey. General Directorate of the Mineral Research and Exploration. Ankara, Turkey 1(2):000
53. Şaroğlu F, Emre Ö, Kuşçu İ (1992) "Türkiye Diri Fay Haritasi (Active fault map of Turkey), scale 1:2000000, one sheet. " in General Directorate of the Mineral Research and Exploration, Ankara
54. Schwartz DP, Coppersmith KJ (1984) Fault behavior and characteristic earthquakes: Examples from the Wasatch and San Andreas fault zones. Journal of Geophysical Research: Solid Earth 89(B7):5681–5698. https://doi.org/10.1029/JB089iB07p05681
55. Şengör AMC, Kidd WSF (1979) Post-collisional tectonics of the Turkish-Iranian plateau and a comparison with Tibet. Tectonophysics 55(3–4):361–376. https://doi.org/10.1016/0040-1951(79)90184-7
56. Şengör AMC (ed) (1980) Türkiye'nin neotektoniğinin esasları. Ankara, Turkey: Türkiye Jeoloji Kurumu (in Turkish). 40s
57. Şengör AMC, Görür N, Şaroğlu F (1985) Strike-slip faulting and related basin formation in zones of tectonic escape: Turkey as a case study.. In: In: Biddle KT, Christie-Blick N (eds) StrikeSlip Deformation, Basin Formation,

and Sedimentation, 1st edn. Special Publications of SEPM, Texas, USA, pp 227–264

58. Şengör AMC, Yazıcı M (2020)) “The aetiology of the neotectonic evolution of Turkey., ” Med Geosc Rev 2:327–339. https://doi.org/10.1007/s42990-020-00039-0
59. Şengör AMC, Grall C, İmren C, Le Pichon X, Görür N, Henry P, Siyako M (2014) The geometry of the North Anatolian transform fault in the Sea of Marmara and its temporal evolution: implications for the development of intracontinental transform faults. Can J Earth Sci 51(3):222–242. https://doi.org/10.1139/cjes-2013-0160
60. Sieh K, Stuiver M, Brillinger D (1989) A more precise chronology of earthquakes produced by the San Andreas fault in southern California. Journal of Geophysical Research: Solid Earth 94(B1):603–623. https://doi.org/10.1029/JB094iB01p00603
61. Taymaz T, Jackson J, McKenzie D (1991) Active tectonics of the north and central Aegean Sea. Geophys J Int 106(2):433–490. https://doi.org/10.1111/j.1365-246X.1991.tb03906.x
62. Thatcher W (1984)) “The earthquake deformation cycle, recurrence, and the time-predictable model., ” Journal of Geophysical Research: Solid Earth 89(B7):5674–5680. https://doi.org/10.1029/JB089iB07p05674
63. Thatcher W (1990) Order and diversity in the modes of circum-Pacific earthquake recurrence. Journal of Geophysical Research: Solid Earth 95(B3):2609–2623. https://doi.org/10.1029/JB095iB03p02609
64. Tsakalos E, Christodoulakis J, & Charalambous L (2016) The dose rate calculator (DRc) for luminescence and ESR dating—A java application for dose rate and age determination. Archaeometry, 58(2), 347-352. https://doi.org/10.1111/arcm.12162
65. Weldon R, Scharer K, Fumal T & Biasi G (2004) Wrightwood and the earthquake cycle: What a long recurrence record tells us about how faults work. GSA today, 14(9), 4-10. https://doi.org/10.1130/1052-5173(2004)014<4:WATECW>2.0.CO;2
66. Wells DL, Coppersmith KJ (1994) New empirical relationships among magnitude, rupture length, rupture width, rupture area, and surface displacement. Bull Seismol Soc Am 84(4):974–1002
67. Wessel P, Smith WH, Scharroo R, Luis J, Wobbe F (2013) Generic mapping tools: improved version released. Eos, Transactions American Geophysical Union 94(45):409–410. https://doi.org/10.1002/2013EO450001

Figures

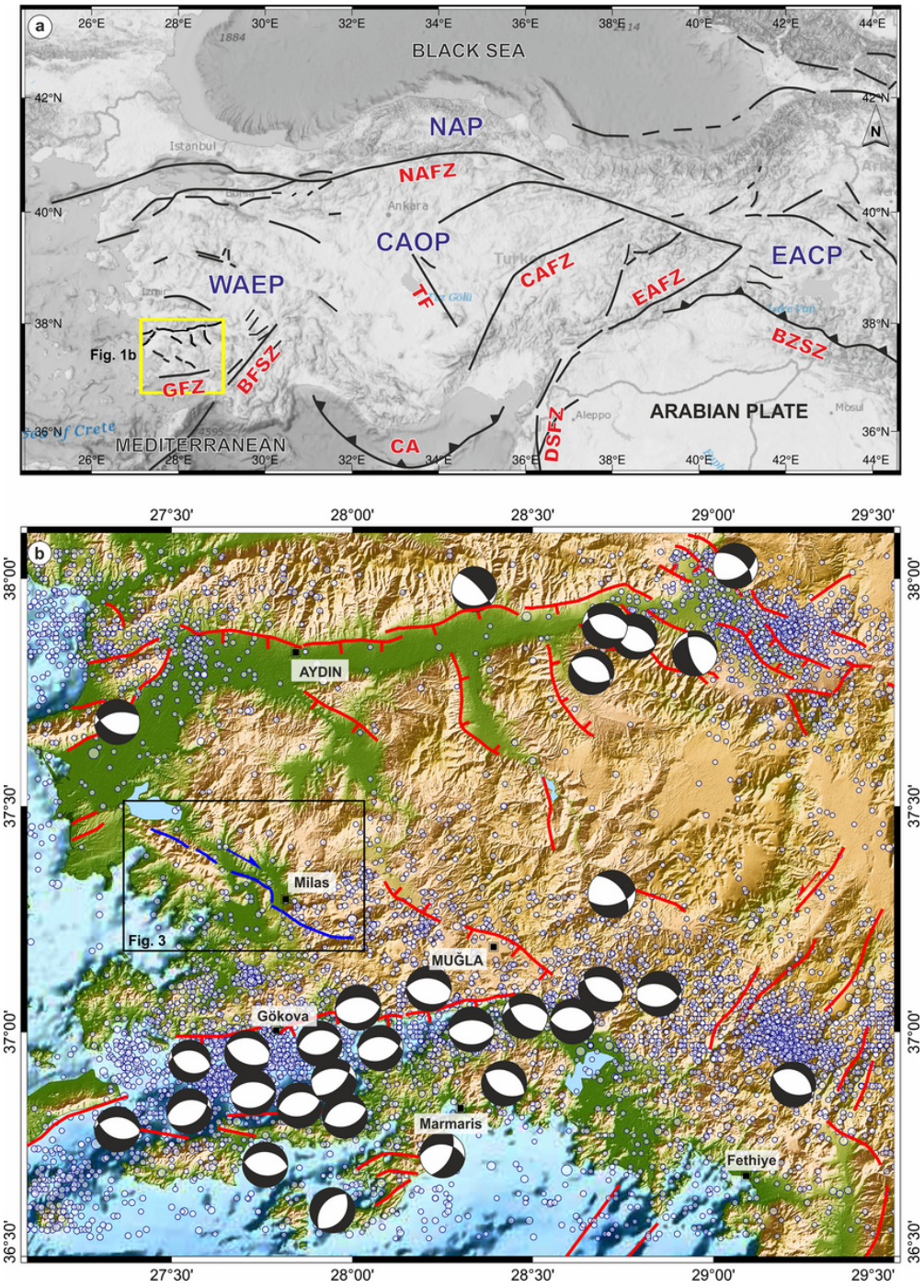

Figure 1

a Major active structure of Anatolia, compiled from (Şengör et al 1985; Barka 1992; Şaroğlu et al 1992; Emre et al 2013; Şengör et al 2014). Key to lettering: CA: Cyprus Arc, CAFZ: Central Anatolian Fault Zone, TF: Tuz Gölü Fault, NAFZ: North Anatolian Fault Zone, EAFZ: East Anatolian Fault Zone, DSFZ: Dead Sea Fault Zone, GFZ: Gökova Fault Zone, BFSZ: Burdur-Fethiye Shear Zone, NAP: North Anatolian Province, EACP: East Anatolian Contractional Province, CAOP: Central Anatolian 'Ova' Province, WAEP: Western Anatolian Extensional Province, BZSZ: Bitlis-Zagros Suture Zone. The base map is the hill shade relief from GEBCO (downloaded from http://www.gebco.net/data_and_products/gridded_bathymetry_data). **b** Seismotectonic map of the SW Turkey (faults are simplified from Emre et al 2013). Blue circles indicate seismic activity ($M_w \geq 3$) between 1900 and 2020 (ISC Earthquake Catalogue). Focal mechanisms ($M_w \geq 4$) downloaded from Global CMT catalog (online)

https://www.globalcmt.org/CMTsearch.html, between 1965 and 2020; and compiled from (Kiratzi & Louvari 2003). The base map is the hill shade relief from ASTER GDEM database (downloaded from http:// https://asterweb.jpl.nasa.gov/gdem.asp)

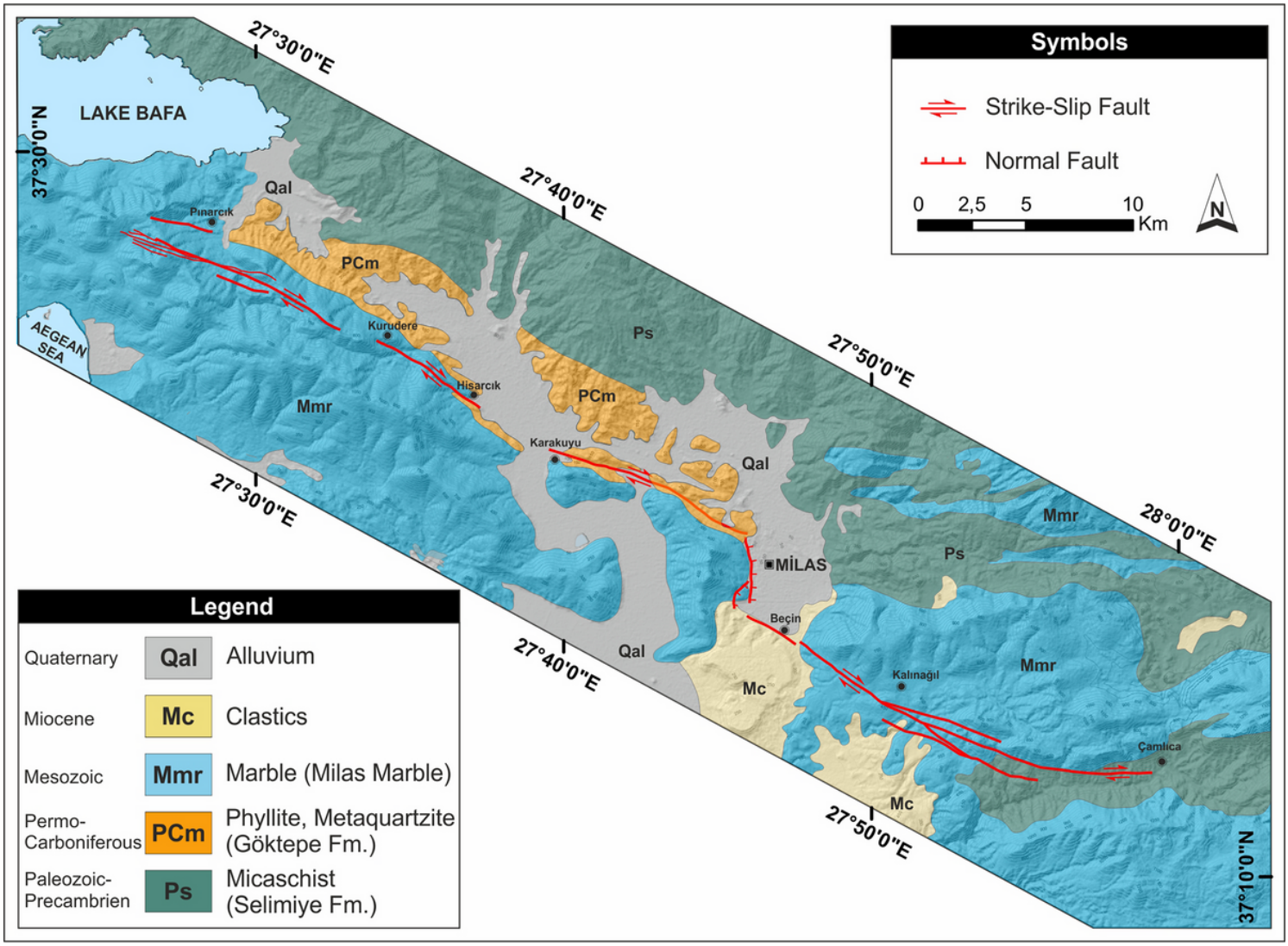

Figure 2

The geological map of Milas Fault and surroundings. Modified and compiled from (Okay 1989; Bozkurt 2007; Akbaş et al 2011; Okay 2008)

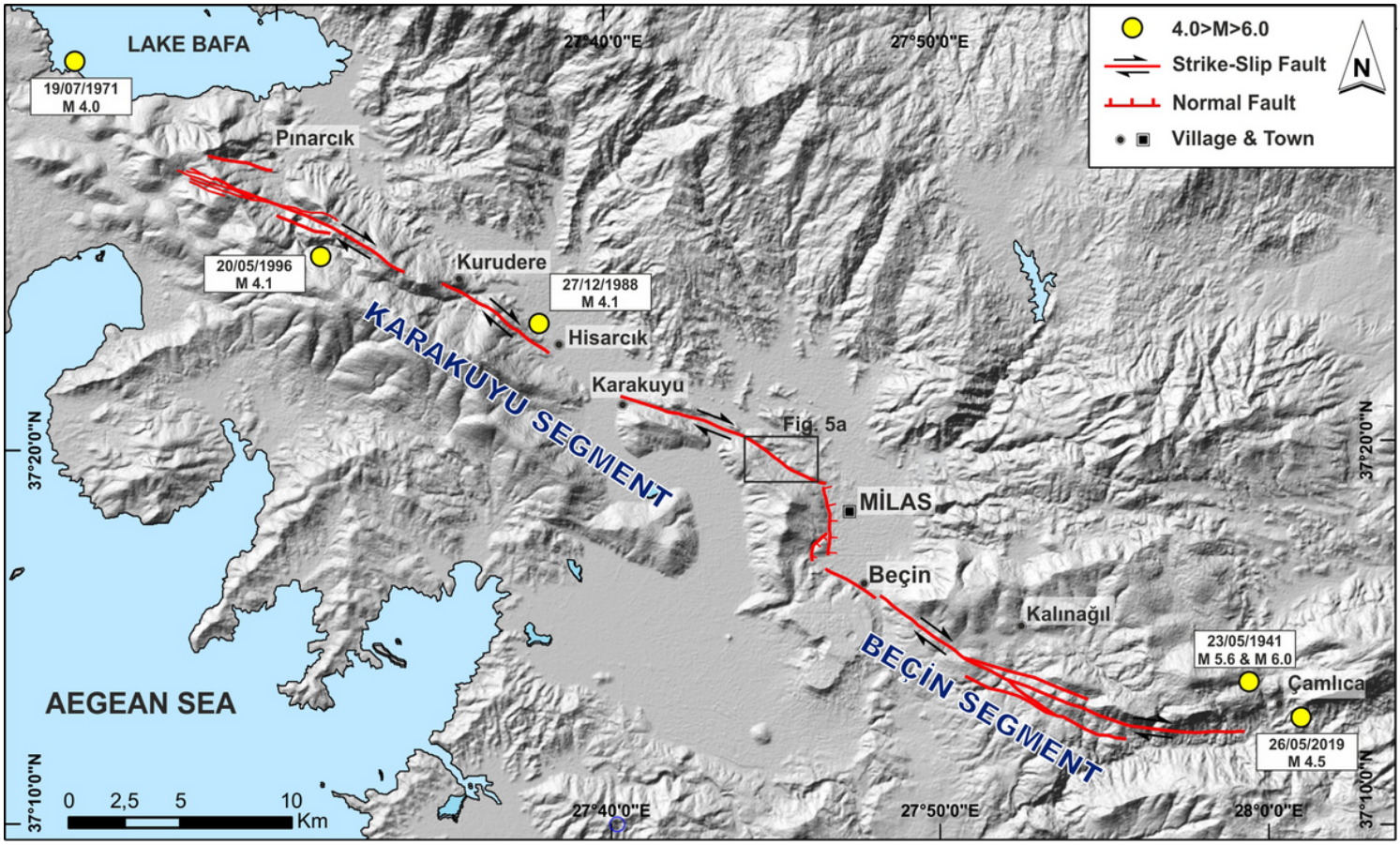

Figure 3

Geometry and segmentation of the Milas Fault and distribution of Mw≥4 earthquakes between 1940 and 2020 (earthquakes data compiled from ISC: International Seismological Centre, NEIC: USGS National Earthquake Information Center, AFAD: Disaster & Emergency Management Authority Presidential of Earthquake Department). The base map is the hill shade relief from ASTER GDEM database

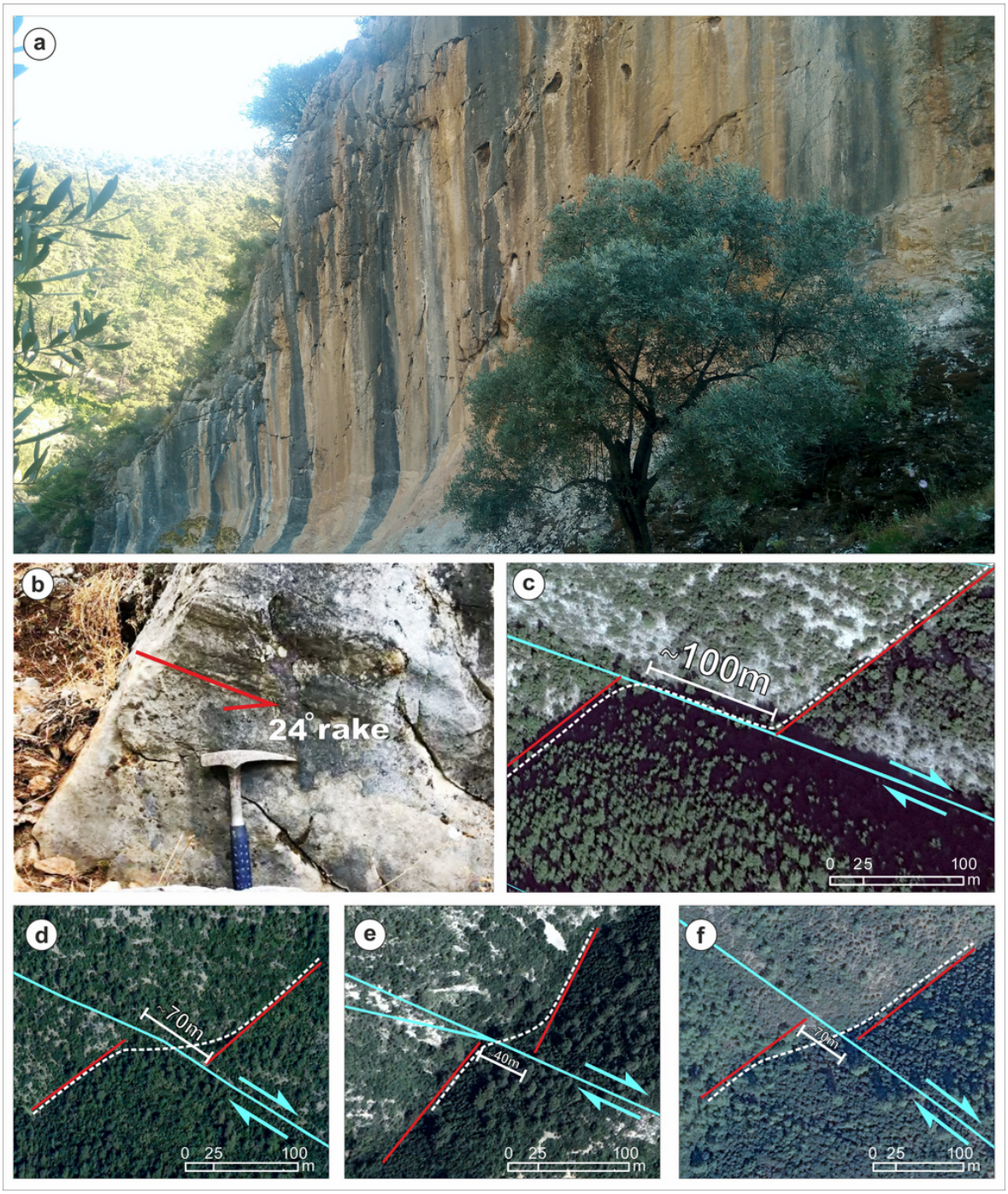

Figure 4

a The fault plane within the limestone unit in the south of the Pınarcık Village (vertical colours are pluvial traces), **b** right-lateral striae with 24° rake angle**. c, d, e, f** show dextrally offset channels (c: 37°26.360'N, 27°28.000'E; d: 37°26.757'N, 27°27.451'E; e: 37°26.093'N, 27°29.363'E; f: 37°23.188'N, 27°36.664'E)

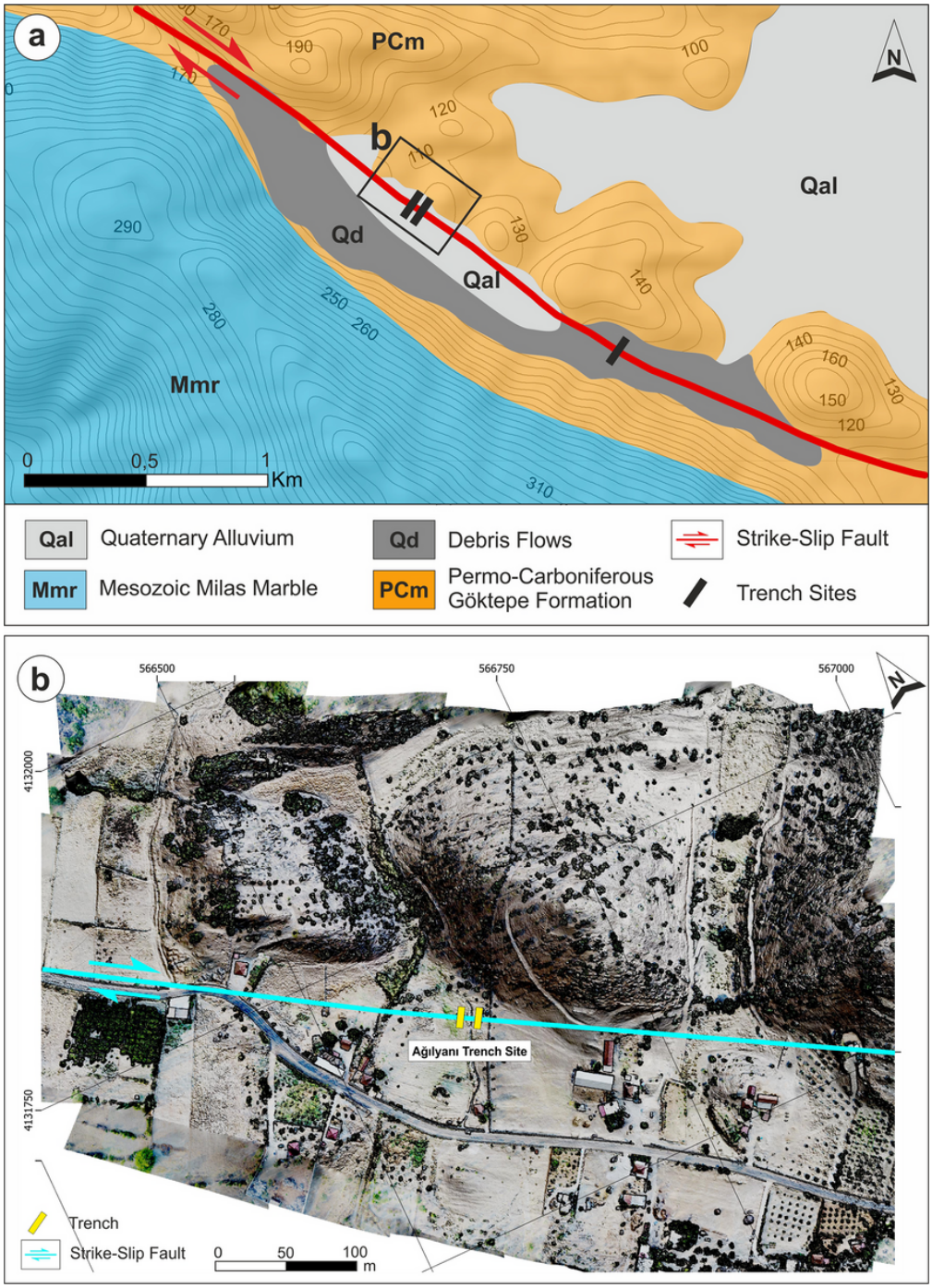

Figure 5

a Geological map showing the Ağılyanı and Zeytinlik trench sites. The region is mainly characterised by Permo-Carboniferous mica schists to the NE and the Mesozoic marbles to the SW in addition to Quaternary alluviums in the middle along the fault-controlled saddle morphology, and **b** UAV-based DSM-Orthophoto representation of the morphology around the Ağılyanı trench site

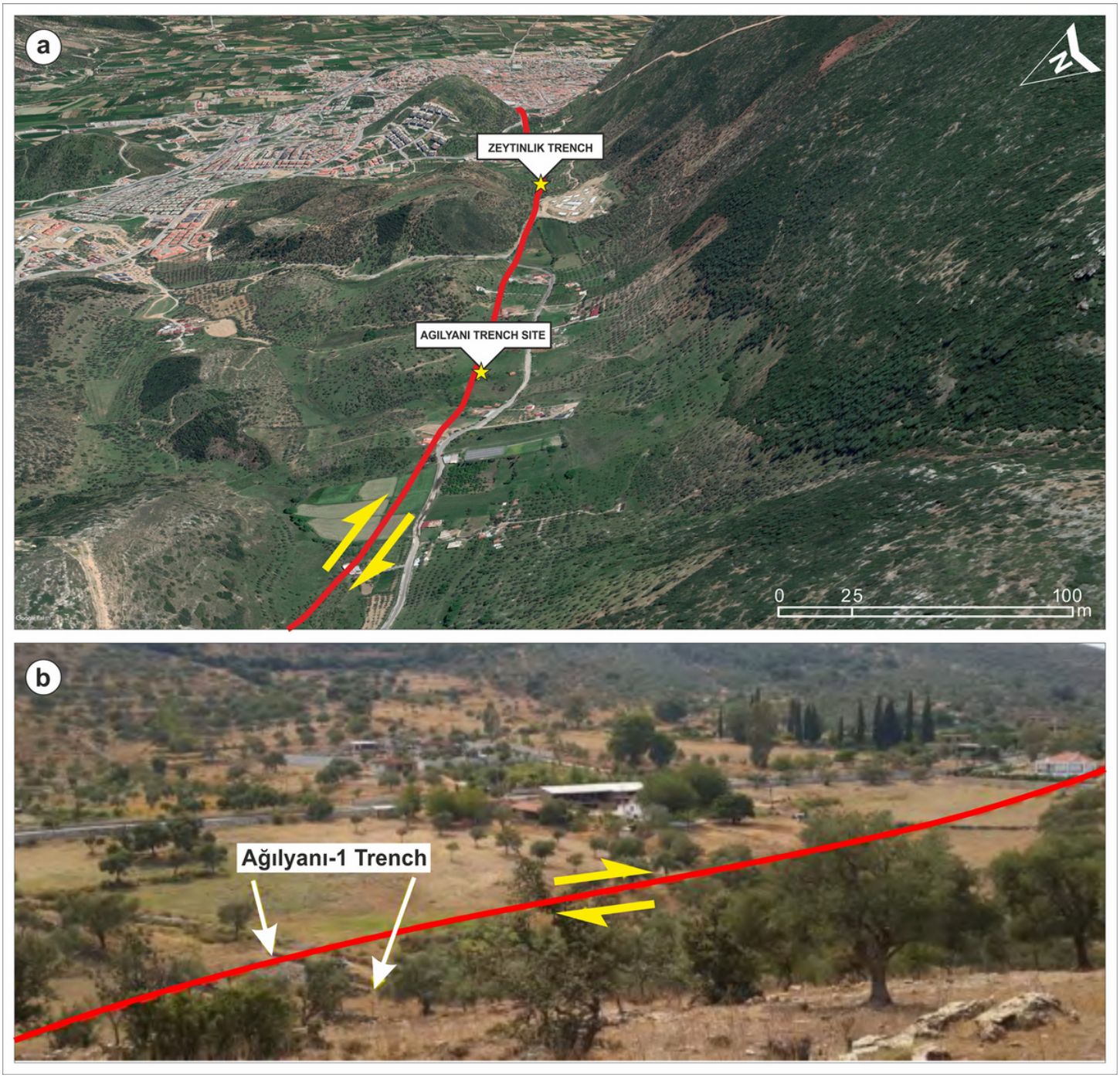

Figure 6

(a) Google Earth image of trench sites on the Karakuyu Segment (X3 vertical exaggeration). (b) Photograph showing the Ağılyanı trench site. The looking direction is to the west

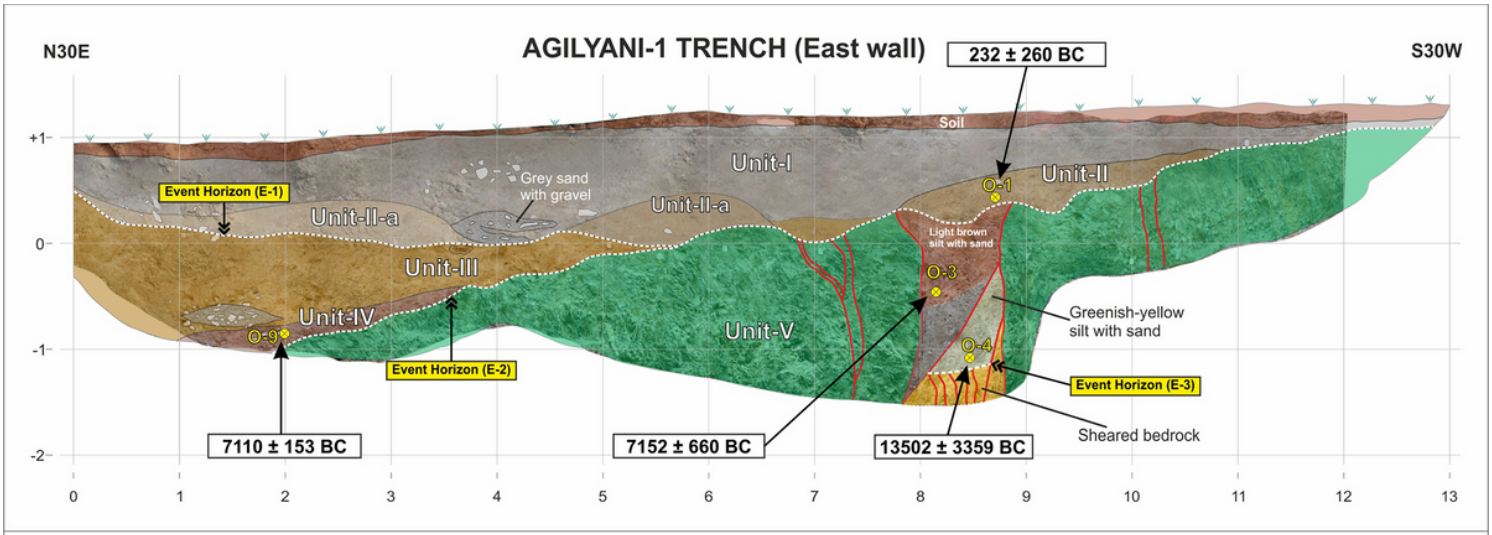

Figure 7

Log of the Ağılyanı-1 Trench (eastern wall). Yellow circles show the locations of OSL samples. Dashed white lines represent event horizons

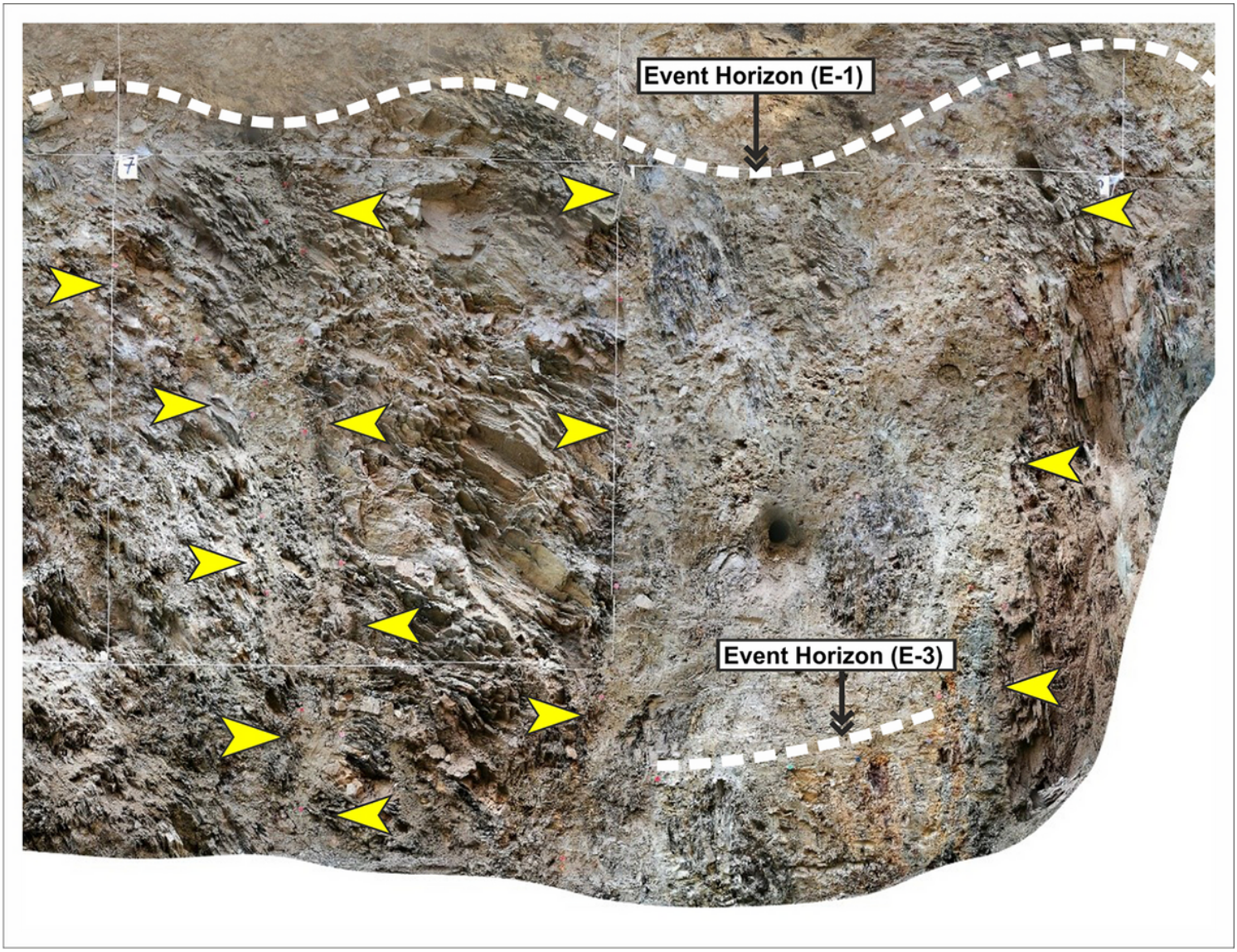

Figure 8

Close-up view of the exposed fault zone between 7th and 9th meters of the Ağılyanı-1 trench. Fault branches are marked with yellow arrows

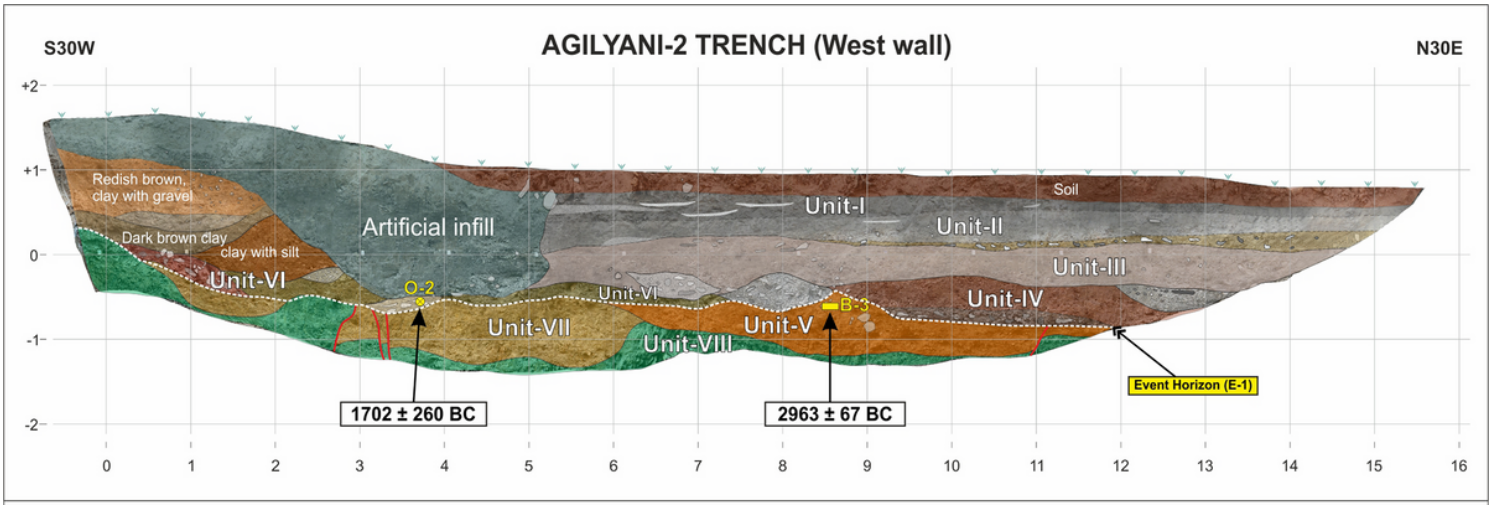

Figure 9

Log of the Ağılyanı-2 Trench (western wall). Yellow circle and rectangle show the locations of OSL and ^{14}C samples, respectively. The dashed white line represents the event horizon

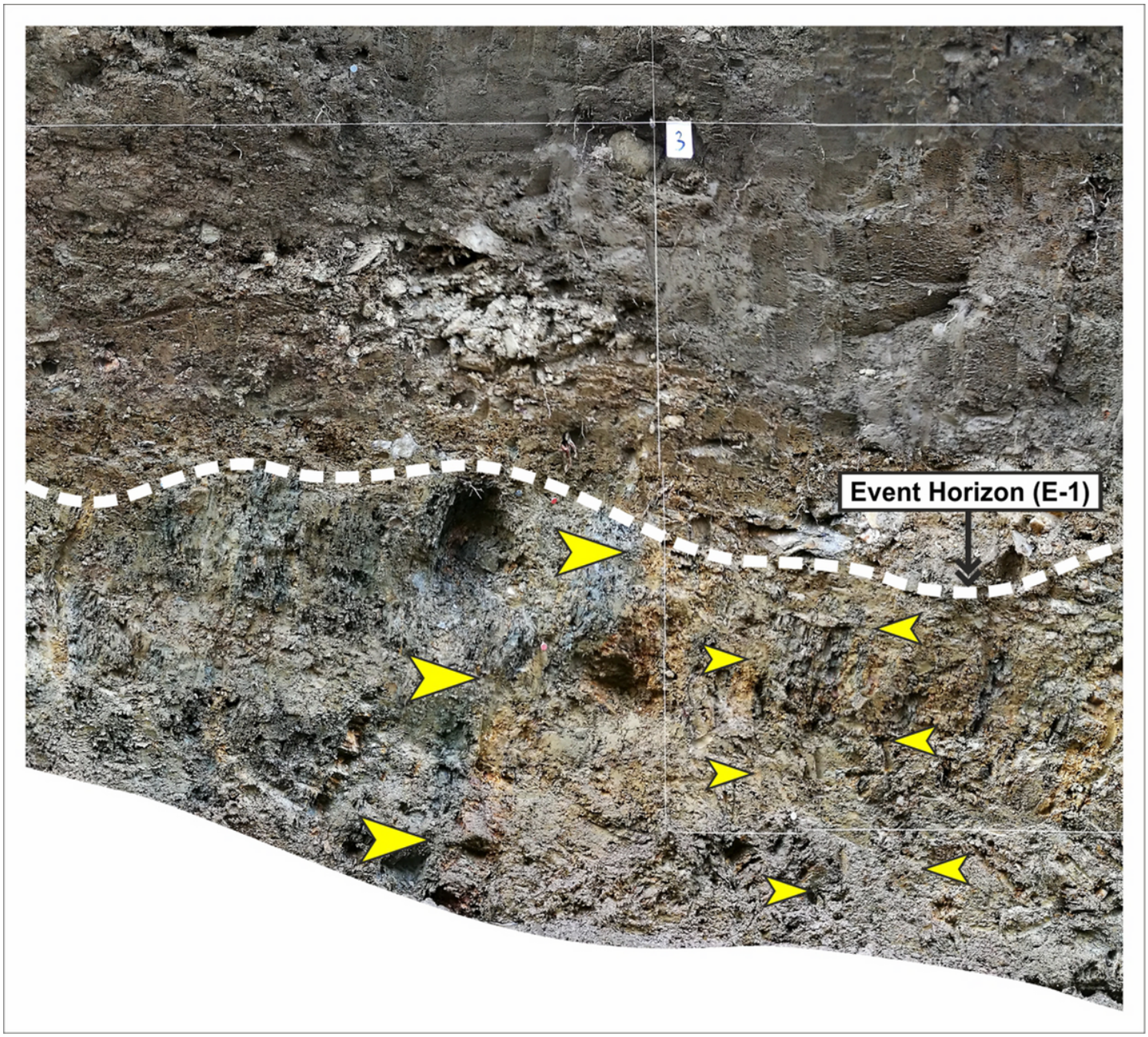

Figure 10

Close-up view of faulting at 2nd and 3rd meters of the Ağılyanı-2 trench. Faults are marked with yellow arrows

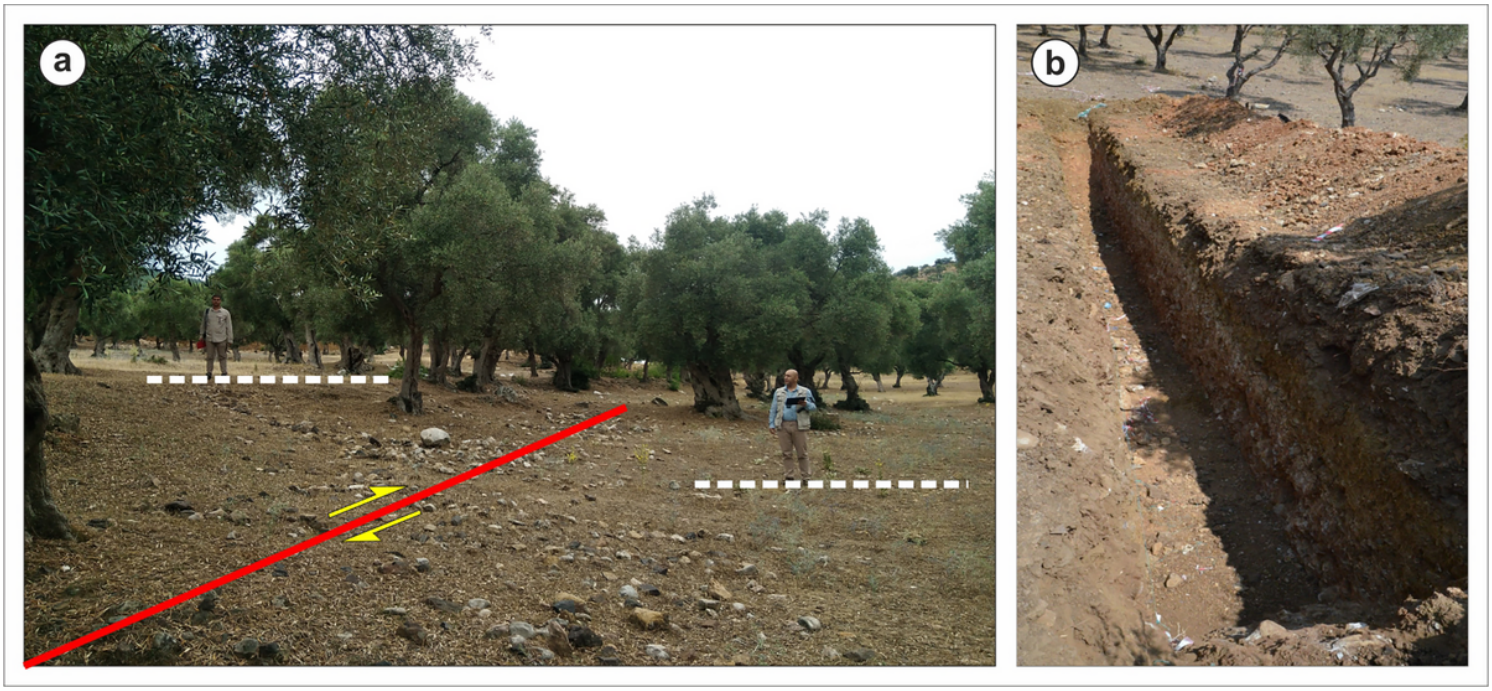

Figure 11

a The linear tectonic scarp with of about 1.5 m height in the Zeytinlik trench site, **b** The Zeytinlik Trench

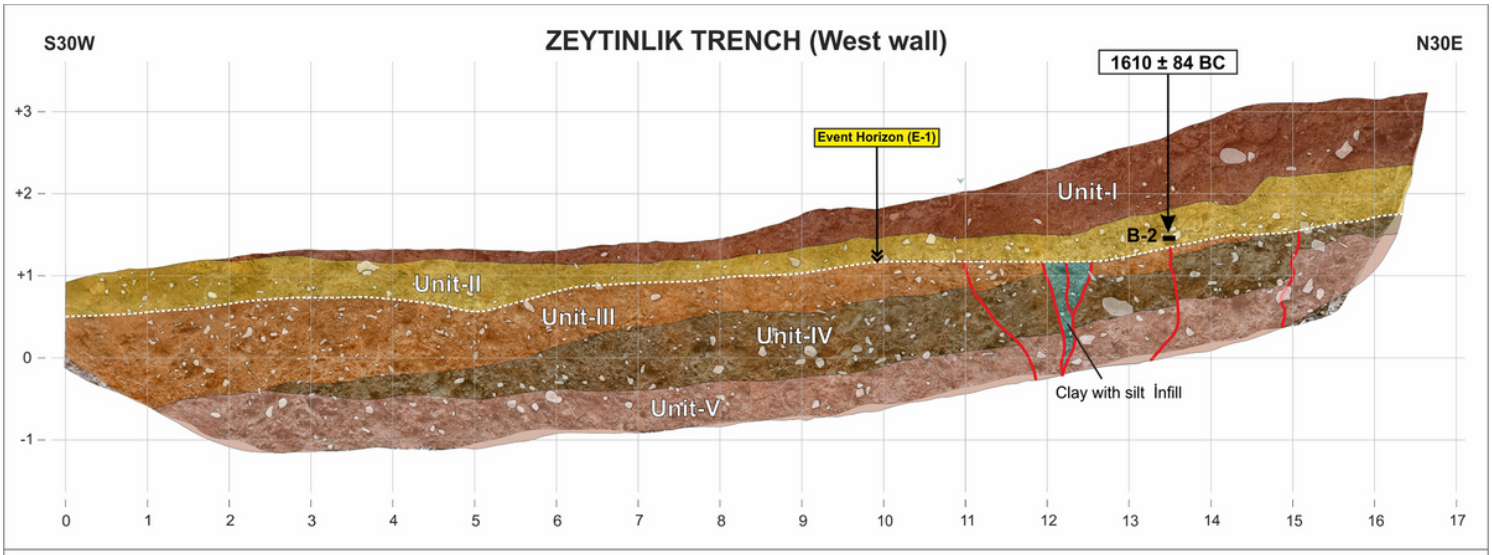

Figure 12

Log of the Zeytinlik Trench (western wall). Black rectangle shows the location of ^{14}C sample

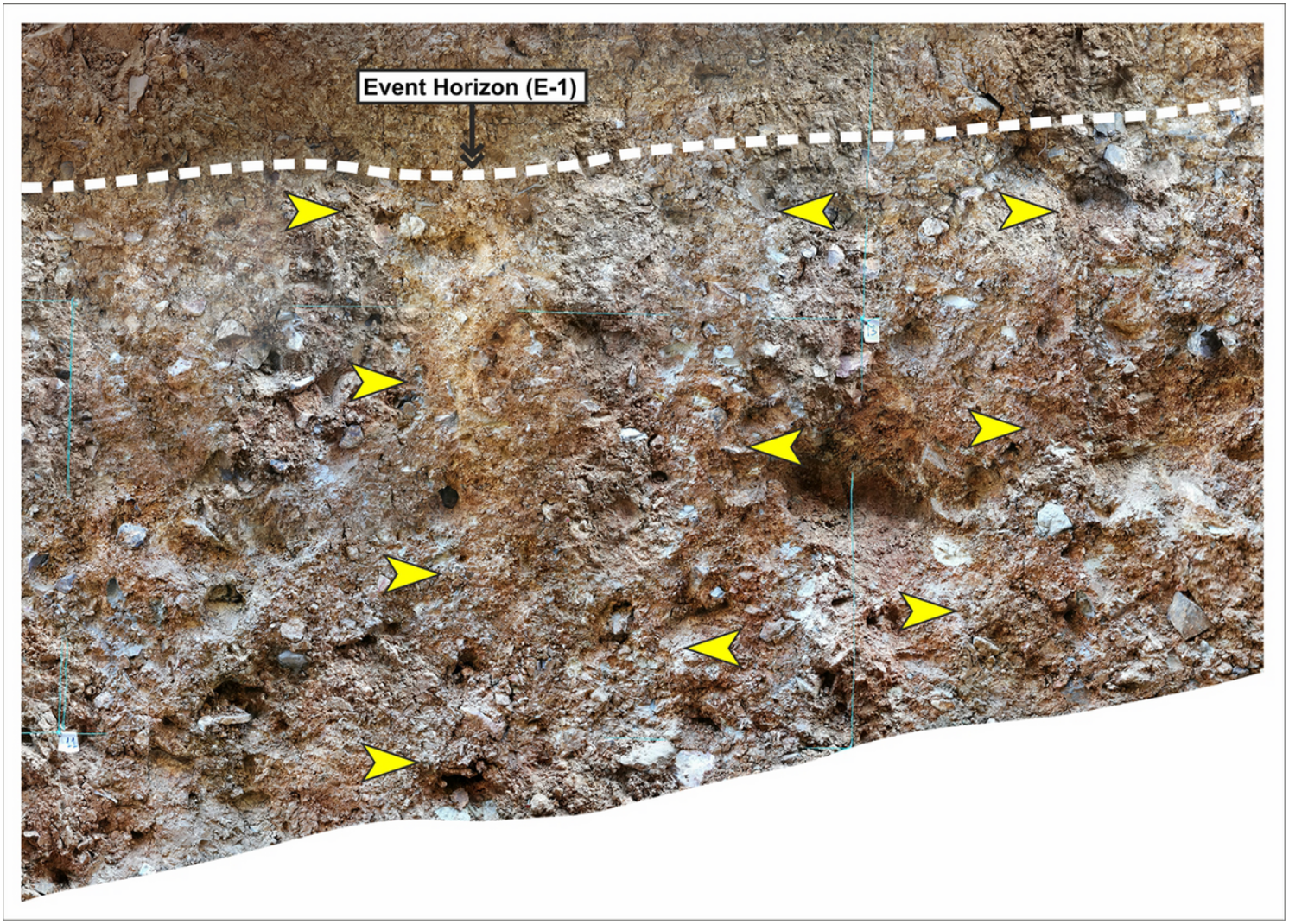

Figure 13

Close-up prospect of the MF from 11th and 14th meters of the of the Zeytinlik trench. Orientation of the fault indicated with yellow arrows

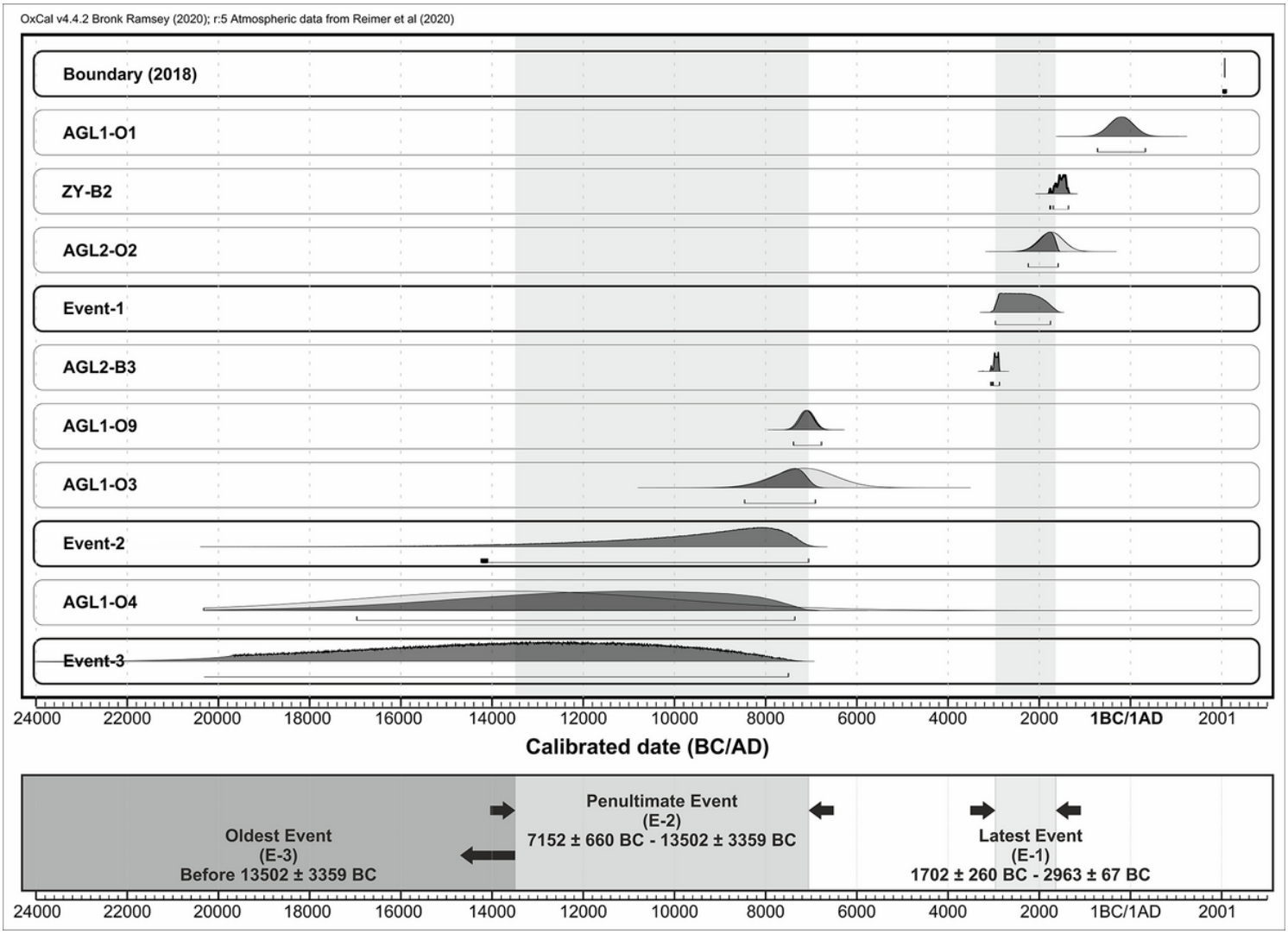

Figure 14

The graph demonstrates the identified events in the Ağılyanı-1, Ağılyanı-2 and Zeytinlik trenches with respect to the probability distribution of radiocarbon and OSL ages (Ramsey & Lee 2013; Ramsey 2020)